Mon. Not. R. Astron. Soc. **367,** 838–850 (2006) doi:10.1111/j.1365-2966.2005.10014.x

Morphology and evolution of simulated and optical clusters: a comparative analysis

Nurur Rahman,[1⋆†‡] Janusz Krywult,[2⋆] Patrick M. Motl,[3⋆] Piotr Flin[2⋆] and Sergei F. Shandarin[1⋆]

[1]*Department of Physics and Astronomy, University of Kansas, Lawrence, KS 66045, USA*
[2]*Institue of Physics, Pedagogical University, Kielce, Poland*
[3]*Department of Physics an Astronomy, Lousiana State University, Baton Rouge, LA 70803, USA*

Accepted 2005 December 16. Received 2005 December 08; in original form 2005 May 12

ABSTRACT

We have made a comparative study of morphological evolution in simulated dark matter (DM) haloes and X-ray brightness distribution, and in optical clusters. Samples of simulated clusters include star formation with supernovae feedback, radiative cooling and simulation in the adiabatic limit at three different redshifts, $z = 0.0, 0.10$ and 0.25. The optical sample contains 208 Abell, Corwin & Olowin (ACO) clusters within redshift, $z \leqslant 0.25$. Cluster morphology, within 0.5 and 1.0 h^{-1} Mpc from cluster centre, is quantified by multiplicity and ellipticity.

We find that the distribution of the DM haloes in the adiabatic simulation appears to be more elongated than the galaxy clusters. Radiative cooling brings halo shapes in excellent agreement with observed clusters; however, cooling along with feedback mechanism makes the haloes more flattened.

Our results indicate relatively stronger structural evolution and more clumpy distributions in observed clusters than in the structure of simulated clusters, and slower increase in simulated cluster shapes compared to those in the observed one.

Within $z \leqslant 0.1$, we note an interesting agreement in the shapes of clusters obtained from the cooling simulations and observation. We also note that the different samples of observed clusters differ significantly in morphological evolution with redshift. We highlight a few possibilities responsible for the discrepancy in morphological evolution of simulated and observed clusters.

Key words: methods: *N*-body simulations – methods: statistical – dark matter – large-scale structure of Universe.

1 INTRODUCTION

The hierarchical clustering is the most popular model for the large-scale structure (LSS) formation. The model relies on the assumption that larger structures result from the merging of smaller subclumps. Theoretical paradigm of the hierarchical evolution is the cold dark matter (CDM) scenario which assumes that baryonic matter (stars, hot X-ray gas) evolves in the dark matter (DM) potential through violent processes. Structural evolution in cosmological objects, such as galaxies or clusters of galaxies, is the underlying principle in this scenario. A generic prediction of the CDM model is the non-sphericity of the DM haloes. The degree of flattening of the haloes evolves in cosmological time, from highly irregular at the distant past towards more regular at the present. In principle, the model prediction can be tested comparing the DM halo shapes with that of the (baryonic) matter distributions. A comparative morphological analysis between model and observation could help constraining the nature of the DM and its role in the LSS.

Melott, Chambers & Miller (2001; hereafter MCM) have reported the evolution in the gross morphology of galaxy clusters (quantified by ellipticity) for a variety of optical and X-ray samples for $z < 0.1$. They infer that the evidence is consistent with a low matter density universe. Using a similar shape measure as well as intracluster medium temperature and X-ray luminosity, Plionis (2002) has presented evidence for recent evolution in optical and X-ray cluster of galaxies for $z \leqslant 0.18$. In both the studies, evolution is quantified by the change of cluster ellipticity with redshift. In a recent study, Jeltema et al. (2005) have reported structural evolution of clusters with redshift where cluster morphology is quantified by the power

⋆E-mail: nurur@kusmos.phsx.ku.edu (NR); krywult@pu.kielce.pl (JK); motl@rouge.phys.lsu.edu (PMM); sfflin@cyf-kr.edu.pl (PF); sergei@ku.edu (SFS)
†Present address: IPAC/California Institute of Technology, Mail Code 100-22, Pasadena, CA 91125, USA.
‡National Research Council (NRC) postdoctoral fellow.

ratio method (Buote & Tsai 1995). Jeltema et al. used a sample of 40 X-ray clusters over the redshift range ~ 0.1–0.8 obtained from *Chandra* Observatory. In spite of methodological differences, the results of these studies indicate evolution in the morphology of the largest gravitationally bound systems over a wide range of look-back time.

The observational evidence prompted concerns about the formation and evolution of structures in the CDM scenario via numerical simulations. If the results of simulations provide faithful representations of the evolutionary history of cosmological objects, then one would expect a similar trend in the structure of simulated objects. So far, almost all studies of simulated clusters are focused on understanding either the nature of the background cosmology within which the present universe is evolving (Jing et al. 1995; Buote & Xu 1996; Crone, Evrard & Richstone 1996; Thomas et al. 1998; Valdarnini, Ghizzardi & Bomometto 1999; Suwa et al. 2003) or the distribution and shape of the DM haloes in various types of simulations, e.g. simulations with or without baryons and gas physics (Dubinski & Carlberg 1991; Dubinski 1994; Aninos & Norman 1996; Tissera & Dominguez-Tenreiro 1998; Bullock 2002; Buote et al. 2002; Jing & Suto 2002; Gao et al. 2004a,b; Kazantzidis et al. 2004; Springel, White & Hernquist 2004; Allgood et al. 2005; Flores et al. 2005; Libeskind et al. 2005; Nagai & Kravtsov 2005; van den Bosch et al. 2005; Zentner et al. 2005; Maccio et al. 2006). Until recently, a comparative study of morphological evolution in simulated and real clusters was absent. Floor et al. (2003) and Floor, Melott & Motl (2004; hereafter FMM) have investigated the evolution in cluster morphology simulated with different initial conditions, background cosmology and different physics [e.g. simulation with or without radiative cooling (RC)]. They have used eccentricity as a probe to quantify evolution. Their studies, emphasizing shape in the outer regions of clusters, suggest slow evolution in simulated cluster shapes compared to the observed one. However, the studies of Floor and collaborators are indirect in a sense that they did not analyse observed clusters using the same measurement technique applied to their simulated data sets.

In this paper, we make a comparative analysis between simulated and observed clusters where both the data sets are juxtaposed and analysed using the same set of structural measures. We analyse cluster morphology and its evolution using shape measures such as multiplicity (M) and ellipticity (ϵ) derived from the Minkowski functionals (Rahman & Shandarin 2003, 2004, hereafter RS03 and RS04; Rahman et al. 2004). The Minkowski functionals (MFs) provide a non-parametric description of the images with no prior assumptions made on the shapes of the images. The measurements based on the MFs appear to be robust and numerically efficient when applied to various cosmological studies, e.g. galaxies, galaxy clusters, cosmic microwave background maps, etc. (Mecke, Buchert & Wagner 1994; Schmalzing et al. 1999; Beisbart 2000; Beisbart, Buchert & Wagner 2001; Beisbart, Valdarnini & Buchert 2001; Kerscher et al. 2001a,b; Shandarin, Sheth & Sahni 2004). Various measures, constructed from the two-dimensional scalar, vector and several tensor MFs, have been described and tested in RS03 and RS04. To derive the parameters applied in this study, we use the extended version of the numerical code developed in RS03 and RS04.

We study evolution in the simulated clusters in a flat CDM universe (ΛCDM; $\Omega_{\rm m} = 0.3$, $\Omega_\Lambda = 0.7$) obtained from three different sets of high-resolution simulations (Motl et al. 2004). The first set has clusters simulated in the adiabatic limit, the second set contains clusters with RC and the last set includes clusters with cooling plus star formation and supernovae feedback (SFF). Each sample contains DM as well as X-ray brightness distributions at three different redshifts, $z = 0.0$, 0.1 and 0.25. For comparison, we also analyse a sample of Abell, Corwin & Olowin (ACO; 1989) clusters within $z \leqslant 0.25$. The sample contains 208 optical clusters derived from 10-inch photographic plates taken with the 48-inch Palomar Schmidt Telescope (Trèvese et al. 1992; Flin et al. 1995; Trèvese et al. 1997; Flin et al. 2000).

The objective of our study is twofold: first, to check the efficiency of the parameters differentiating various sets of objects and, secondly, to explore (statistical) correspondence in the morphological properties of the distributions of DM haloes, X-ray emitting gas and optical clusters using measures that are sensitive to shape and substructures.

In the CDM model (satellite), galaxies are associated with the DM subhaloes that are accreted by their (current) parent halo, a bigger structure usually associated with a galaxy cluster. If this is the case, statistical properties of galaxies regarding mass, substructure, shape, etc., would show a similar trend to that of the subhaloes. On the other hand, X-ray emitting hot gas, evolving in the DM background potential, would not directly follow the DM distribution because of its isotropic pressure support. Therefore, a statistical analysis of various properties of DM haloes, galaxy clusters and X-ray gas distributions will be useful to probe possible bias of luminous galaxies towards subhaloes and their correspondence with the distribution of hot gas. This is the motivation behind the second objective.

The organization of the paper is as follows. Simulation technique and the observational data are described briefly in Section 2, and a brief discussion of shape measures is given in Section 3. The results are presented in Section 4 and the conclusions are summarized in Section 5.

2 DATA

2.1 Numerical Simulations

We have analysed images of simulated clusters projected along three orthogonal axes. The clusters have been simulated in the standard, flat CDM universe (ΛCDM) with the following parameters. $\Omega_{\rm b} = 0.026$, $\Omega_{\rm m} = 0.3$, $\Omega_\Lambda = 0.7$, $h = 0.7$ and $\sigma_8 = 0.928$. For a complete description of the simulations, see Motl et al. (2004). We have used three samples of clusters derived from the same initial conditions and background cosmology. The difference between the samples is in the energy loss mechanism experienced by the baryonic fluids. In the first sample, no energy lose is allowed; in the second sample, fluid is allowed to lose energy via radiation and subsequently cool; and in the third sample, physics of SFF are incorporated in addition to RC.

The simulations use a coupled N-body Eulerian hydrodynamics code (Norman & Bryan 1999) where the DM particles are evolved by an adaptive particle mesh, N-body code. The piecewise parabolic method (PPM) scheme (Colella & Woodward 1984) is used to treat the fluid component on a comoving grid. An adaptive mesh refinement (AMR) is employed to concentrate the numerical resolution on the collapsed structures that naturally form in cosmological simulations. The DM particles exist on the coarsest three grids; each subgrid having twice the spatial resolution in each dimension and eight times the mass resolution relative to its parent grid. At the finest level, each particle has a mass of $9 \times 10^9\, h^{-1}\, {\rm M}_\odot$. A second-order accurate triangular-shaped cloud (TSC) interpolation is used for the adaptive particle mesh algorithm. Up to seven levels of refinement are utilized for the fluid component, yielding a peak resolution of $15.6\, h^{-1}$ kpc within the simulation box with sides of length $256\, h^{-1}$

Mpc at the present epoch. Clusters are selected using the HOP algorithm (Eisenstein & Hut 1998) with an overdensity threshold of 160.

A tabulated cooling curve (Westbury & Henriksen 1992) for a plasma of fixed, 0.3 solar abundance has been used to determine the energy loss to radiation. Heat transport by conduction is neglected in the present simulations since it has been shown that even a weak, ordered magnetic field can reduce conduction by two to three orders of magnitude from the *Spitzer* value (Chandran & Cowley 1998). However, Narayan & Medvedev (2001) have shown that if the chaotic magnetic field fluctuations extend over a sufficiently large length-scales within the intracluster medium (ICM), then thermal conductivity becomes significant to the global energy balance of the ICM. Energy input into the fluid from active galactic nucleus (AGN) is also neglected in the current simulations.

The prescription of Cen & Ostriker (1992) has been used to transform collapsing and rapidly cooling gas into collisionless star particles. At the finest resolution level, a grid cell is eligible to form a star in a given time-step if the local flow is converging, the dynamical time exceeds the cooling time and a Jeans mass worth of gas exists within the cell. To model a population of prompt supernovae, thermal feedback has been introduced. The amount of feedback has been set from numerical experiments to provide a reasonable amount of mass in star particles. The feedback is approximately 7×10^{48} erg per solar mass of stars formed or about half a keV of energy per particle in the final clusters.

We have 41 three-dimensional clusters from each sample, giving a total of 123 projected clusters in the respective samples. Each projection is constructed within an $8\ h^{-1}$ Mpc (comoving) frame containing 360×360 pixels. Majority of clusters in each sample is in the mass range $\sim 10^{13}$–$10^{14}\ \mathrm{M}_{\odot}$ with a few clusters ($\sim$15) in the limit $\sim 10^{15}\ \mathrm{M}_{\odot}$.

2.2 Optical clusters

The details of data acquisition and processing of the optical sample have been described in Trèvese et al. (1992), Flin et al. (1995), Trèvese et al. (1997) and Flin et al. (2000). Here, we highlight only the essential features of the sample needed for this study.

The sample contains 208 optical clusters, within $z \leqslant 0.25$, derived from 10-inch photographic plates taken with the 48-inch Palomar Schmidt Telescope. It contains rich and massive ACO clusters with richness $R \geqslant 1$ and mass, approximately, in the range $\sim 10^{13}$–$10^{14}\ \mathrm{M}_{\odot}$. Highly massive structures, e.g. Coma cluster (A1654) or clusters constituting the Shapley condensation, are absent in this sample.

The visual control is the greatest advantage of this sample. The essential difference between this and other samples is visual control of all objects classified as galaxies when automatic procedure was applied. The visual inspection was done for objects with magnitude range at least $m_3 + 3$ mag. The relationship between the number of objects with respect to the magnitude and the luminosity function for each separate cluster shows that clusters are complete at least in the magnitude range m_3 to $m_{2.5}$. In the majority of cases, it is complete till $m_3 + 3$.

3 MORPHOLOGICAL PARAMETERS

We use multiplicity (M) and ellipticity (ϵ) as quantitative measures to study evolution of observed and simulated clusters. Ellipticity is derived from the area tensor functional, a member of the hierarchical set of the MFs. This functional is given by

$$A_{ij} = \int_K (x_i - A_i)(x_j - A_j)\,\mathrm{d}a, \tag{1}$$

where K is the region bounded by a given contour and A_i is the area vector functional, i.e. area centroid, expressed as

$$A_i = \frac{1}{A_S} \int_K x_i\,\mathrm{d}a. \tag{2}$$

The symbol A_S represents the area within the contour. It is known as the scalar area functional and is given by

$$A = \int_K \mathrm{d}a. \tag{3}$$

The area vector functional is, in fact, the centre of mass of the region within the contour if we assume that the surface density of the (enclosed) region is constant. The area tensor functional is closely related to the inertia tensor of a homogeneous region. The details of the MFs can be found in Schmalzing (1999), Beisbart (2000) and RS03.

(i) Multiplicity (M): this parameter is defined as

$$M = \frac{1}{A_{\max}} \sum_{i=1}^{N} A_i = \frac{A_S}{A_{\max}}, \tag{4}$$

where A_i is the area of the individual components at a given level, $A_{\max}$ is the area of the largest component at that level, N is the total number of components and A_S is the total area at that level obtained after summing the areas of the components. Multiplicity, $M = M(A_S)$, is a measure with fractional value and gives the number of components measured at any brightness level: $M = 1$ for a single iso-intensity contour, i.e. component, and $M > 1$ for multicontours.

It may be mentioned here that Thomas et al. (1998) have used multiplicity as a parameter for substructure measure in N-body simulations. They define it as a ratio of mass of subclumps to cluster mass. In this study, it is a ratio of the areas (sizes) as defined in equation (1).

We use two variants of M to present our results: one is the average of multiplicity over all density/brightness levels, $\bar{M}_{\mathrm{eff}}$, and the other is the maximum of the multiplicity found at one of the levels, $M_{\max}$.

(ii) Ellipticity (ϵ): we adopt the definition of ellipticity,

$$\epsilon = 1 - b/a, \tag{5}$$

where a and b are the semi-axes of an ellipse. For our purpose, the semi-axes correspond to the 'auxiliary ellipse' constructed from the eigenvalues of the area tensor (see RS03 for detail). Note that the 'auxiliary ellipse' is an ellipse having exactly the same area tensor.

We have used two variants of ϵ: one is sensitive to the shape of the individual cluster components present at a given level while the other is sensitive to the collective shape formed by all the components present at that level. We label these two variants of ϵ, respectively, as the effective (ϵ_{eff}) and the aggregate (ϵ_{agg}) ellipticity. Morphological properties of clusters, such as shape and the nature or the degree of irregularity existing in these systems, can be probed effectively with these two parameters.

At any given density/brightness level, we construct ϵ_{eff} as a weighted mean normalized by the multiplicity and area of the largest contour,

$$\epsilon_{\mathrm{eff}} = \frac{1}{M A_{\max}} \sum_{i=1}^{N} \epsilon_i A_i, \tag{6}$$

where ϵ_i are ellipticities of the individual components measured as stated earlier and M is the multiplicity at that level. The symbols A_i and $A_{\max}$ have similar meanings as before. This measure can be used as an effective tool to quantify shapes of large-scale merger remnants.

To construct $\epsilon_{\rm agg}$, we take the union of all components present at a given level and form a collective region. The integrated region can be expressed as

$$R = R_1 \cup R_2 \cup \cdots \cup R_N, \tag{7}$$

where R_i is the region enclosed by each contour. Subsequently, we find the components of the area tensor and the 'auxiliary ellipse' for the region R.

The behaviour of $\epsilon_{\rm agg}$ is similar to the conventional ellipticity measure based on the inertia tensor (Carter & Metcalfe 1980). But, the construction procedure of these two measures is different. The conventional method finds the eigenvalue of the inertia tensor for an annular region enclosing mass density or surface brightness. On the other hand, the method based on MFs finds the eigenvalues of regions enclosed by the contour(s) where the regions are assumed to be homogeneous.

We have computed ellipticities after averaging the estimates at all density/brightness levels. Our final result is, therefore, expressed as $\bar{\epsilon}_{\rm eff}$ and $\bar{\epsilon}_{\rm agg}$.

3.1 Toy models

To get a better feeling of the parameters mentioned above, we provide an illustrative example with toy models. We find this demonstration useful since it gives a visual expression about how the number of group members forming complex structures affects the shapes (see also Paz et al. 2006).

One can think of these toy images as snapshots of different clusters (in projection) taken at one particular time. We include clusters with different types of internal structures in Fig. 1: unimodal elliptic structure (Panel 1), asymmetric and symmetric bimodal clusters (Panels 2 and 3, respectively), cluster with filamentary structure (Panel 4), etc. The multimodal clusters have clumps with different

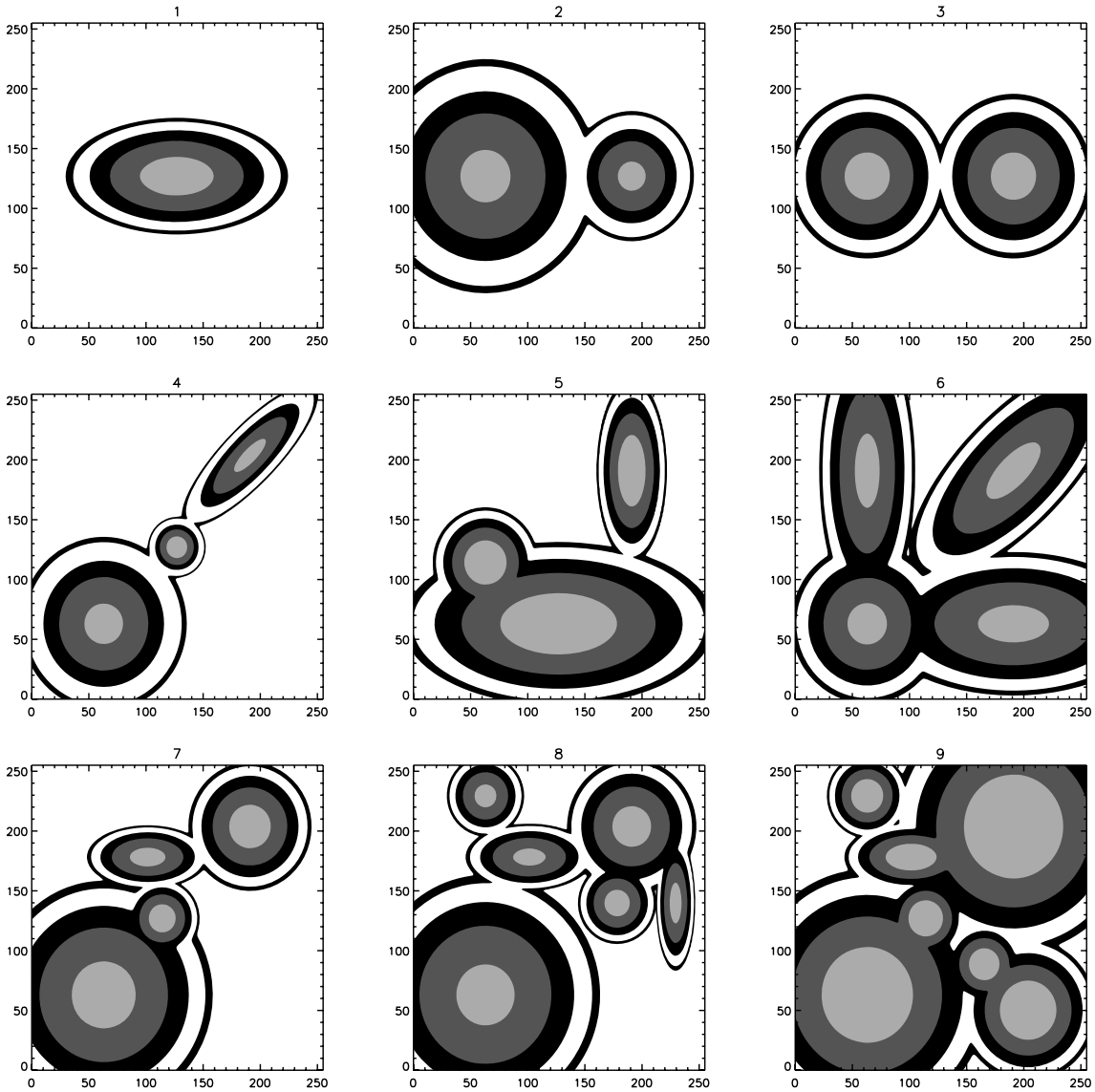

Figure 1. Contour plots of toy clusters at different brightness levels (in arbitrary scales). The multimodal clusters have clumps with different peak brightness. For all clusters, the outer line represents the percolation level where the substructures merge and form a single, large system.

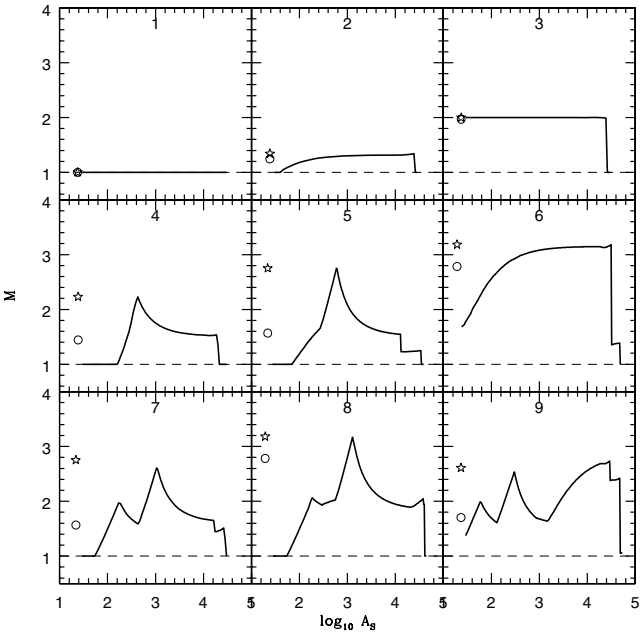

Figure 2. Multiplicity as a function of contour area (A_S) for toy clusters as shown in Fig. 1. The circle (star) represents the effective multiplicity $\bar{M}_{\rm eff}$ (maximum multiplicity $M_{\rm max}$) as defined in the text. The x-coordinates of these legends are chosen only for the convenience of demonstration. Recall that the position of the highest peak along the x-axis corresponds to the $M_{\rm max}$ whereas $\bar{M}_{\rm eff}$ is obtained after averaging along the x-axis. See text for details.

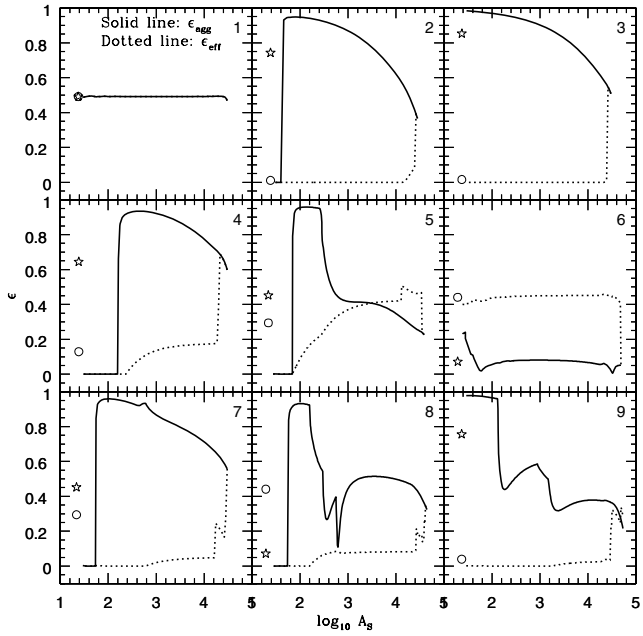

Figure 3. Ellipticity as a function of contour area (A_S) for toy models as shown in Fig. 1. Dotted and solid lines represent, respectively, $\epsilon_{\rm eff}$ and $\epsilon_{\rm agg}$. The circle (star) represents the $\bar{\epsilon}_{\rm eff}$ ($\bar{\epsilon}_{\rm agg}$) for these toy clusters as defined in the text. Once again, the x-coordinates of these legends are chosen only for the convenience of demonstration. See text for details.

peak brightness. We show contour plots of toy clusters at different brightness levels where the levels are chosen arbitrarily. For all clusters, the outer line represents the percolation level where the substructures merge with one another and form a single, large system.

Multiplicity as a function of component area (in grid units) is shown in Fig. 2 for our selected toy models. As mentioned earlier, M is sensitive to the size of the substructures. The simplest case to see this is a bimodal cluster. For a bimodal structure with unequal subclumps (Panel 2), the fractional value of multiplicity ($1 < M < 2$) tells us that the components of the system have different sizes. The isolated components eventually percolate giving $M = 1$ at low brightness level, i.e., at larger area. On the other hand, for a cluster with equal components $M = 2$ until percolation occurs (Panel 3). For clusters with three components (Panels 4 and 5), we see that for a small range of brightness levels, the components are well separated where two of these are bigger then the third one ($2 < M < 3$). Afterwards, two of the three clumps merge together giving $1 < M < 2$. These two remaining components eventually percolate to become a single system. The clumps in Panel 6 are distributed around the centre. For this cluster, we see two unequal but well-separated clumps ($1 < M < 2$) with the same peak brightness. The behaviour of clusters in Panels 7 and 8 is similar except that they have a different number of substructures. The cluster in Panel 9 has the largest number of components (a total of seven). Two of its clumps are so large compared to the other ones that they dominate. The multiplicity is always in the range $1 < M < 3$, reflecting the merger of clumps at different levels.

Ellipticity for these toy clusters is shown in Fig. 3. In this figure, the solid and dotted line represent, respectively, $\epsilon_{\rm agg}$ and $\epsilon_{\rm eff}$. For the unimodal cluster in Panel 1, $\epsilon_{\rm eff} = \epsilon_{\rm agg}$. For the bimodal cluster in Panel 2, the estimate of $\epsilon_{\rm eff}$ is weighted more by the larger component. It is zero for the case shown in Panel 2. This is also true for the cluster in Panel 3. However, for a bimodal system with equal-sized subclumps but different elongation, $\epsilon_{\rm eff}$ will give an average elongation of the two. For systems with substructures, the estimate of $\epsilon_{\rm agg}$, on the other hand, tells us about the overall shape of these systems. Due to the presence of two isolated components, the system itself appears more elongated than the shape of its subclumps. An important point to note is that the estimate provided by $\epsilon_{\rm agg}$ depends not only on the relative sizes of the components but also on their relative separations. This is reflected in the panels containing multiclump clusters. For equal separation, a bimodal cluster with components similar in shape but unequal in size has lower $\epsilon_{\rm agg}$ than that of a bimodal cluster with identical shape and size (see the region $1.8 < \log_{10} A_S < 2.2$ in Panels 2 and 3 in Fig. 3). In general, as the density and brightness level decrease the clumps get bigger and appear closer to one another, and $\epsilon_{\rm agg}$ gets smaller.

Note that for a multicomponent system with filamentary structure, $\epsilon_{\rm eff} < \epsilon_{\rm agg}$ (Panel 4). On the other hand, if components are distributed around the cluster centre, $\epsilon_{\rm eff} > \epsilon_{\rm agg}$ (Panel 6). The cluster in Panel 5 has the unique property that is shown separately by clusters in Panels 4 and 6. In transition at a lower brightness level, the cluster changes its filamentary shape to an extended structure where the components are distributed over a region around the centre. The $\epsilon_{\rm agg}$ profile in Panel 8 shows that in the range, $2.2 < \log_{10} A_S < 2.8$, the cluster develops two, almost equal size clumps that are very close to each other. The cluster in Panel 7 follows the behaviour of a bimodal cluster except that there is jump in between $2.6 < \log_{10} A_S < 2.8$ where the cluster changes its structure having two unequal size clumps to two equal size clumps. The shape of the cluster in Panel 9 changes consistently following the merger of its clumps at different brightness levels.

In Figs 2 and 3, we also show the variants of the parameters used later in this study. We use circle and star to represent the structural parameters, $\bar{M}_{\rm eff}$ and $M_{\rm max}$. The respective symbols are also used for the shape parameters $\bar{\epsilon}_{\rm eff}$ and $\bar{\epsilon}_{\rm agg}$. Comparing this set of parameters with more general M and ϵ, one can easily see how these measures response to the alignment of substructures and their spatial locations (filamentary, extended, etc.).

3.2 Example of simulated clusters

We demonstrate the behaviours of M and the variants of ϵ as a function of area for a collection of simulated clusters in Figs 4 and 5. For each sample, we choose two clusters at each redshift. We use dark, grey and faint solid lines to represent, respectively, the adiabatic, RC and SFF samples. The DM haloes and X-ray clusters are shown on the left- and right-hand panels, respectively.

Fig. 4 shows that both matter and X-ray clusters with cooling, generally, have a higher number of subclumps than those without cooling. Fig. 5 shows that in most cases the central part of cluster consists of a single peak ($\epsilon_{\rm eff} = \epsilon_{\rm agg}$). The central region of these clusters does not appear spherical, rather this region has some degree of flattening. We see that multipeak systems, mostly bimodal clusters with unequal size subclumps ($\epsilon_{\rm eff} < \epsilon_{\rm agg}$), are common for these clusters. At low brightness levels, i.e. in the outer regions of clusters, the subclumps appear in various shapes. In some cases, they merge forming one system ($\epsilon_{\rm eff} = \epsilon_{\rm agg}$), in a few cases they appear homogeneously distributed ($\epsilon_{\rm eff} > \epsilon_{\rm agg}$), and in a few cases they form filamentary structure ($\epsilon_{\rm eff} < \epsilon_{\rm agg}$). The degree of inhomogeneity ($\epsilon_{\rm eff} \neq \epsilon_{\rm agg}$), generally, is higher for X-ray clusters. There is a weak trend that cluster centres are more flattened than the outer parts, irrespective of the nature of simulation.

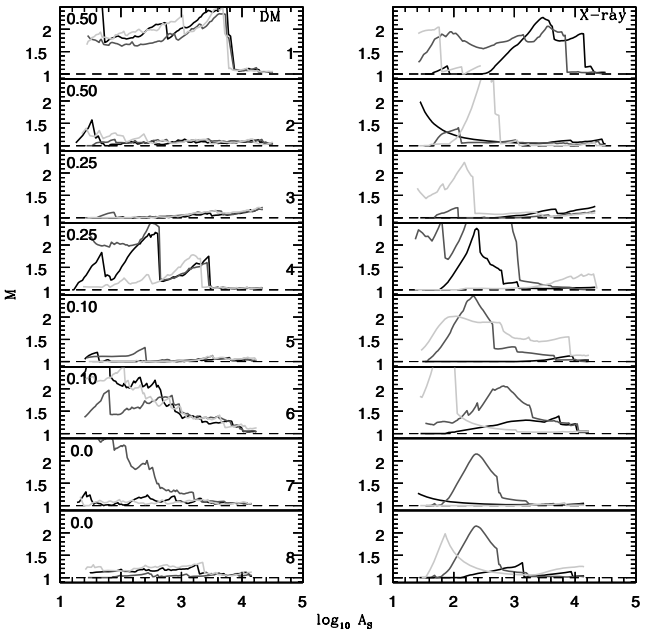

Figure 4. Multiplicity (M) as a function of contour area (A_S) for a selection of clusters at $z = 0.50, 0.25, 0.10$ and 0.0. Two clusters from each redshift are shown. Dark, grey and faint solid lines represent, respectively, the adiabatic, RC and star formation with feedback (SFF) samples. The DM and X-ray clusters are shown on the left- and right-hand panels, respectively. Multiplicity is, in general, greater than 1 in the entire redshift range for clusters simulated with RC (medium line) indicating a slower evolution than in the adiabatic sample (dark line). Redshift $z = 0.5$ is taken for demonstration purpose only. See text for details.

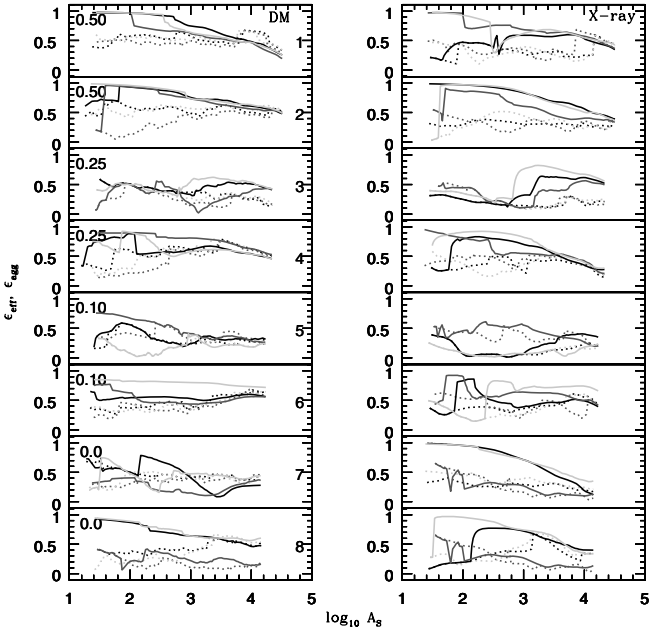

Figure 5. Effective ($\epsilon_{\rm eff}$) and aggregate ($\epsilon_{\rm agg}$) ellipticity as a function of contour area (A_S) for the same clusters as in Fig. 4. Solid and dotted lines are used to represent $\epsilon_{\rm agg}$ and $\epsilon_{\rm eff}$, respectively. The colour style is similar to Fig. 4. In most cases, the non-spherical central part of these clusters consists of a single peak (i.e. $\epsilon_{\rm eff} = \epsilon_{\rm agg}$) whereas in the outer regions subclumps show various shapes. It can be seen easily that the central regions of clusters in hydrodynamic simulations appear to be more regular. We note that cluster centres are slightly more flattened than the outer parts, irrespective of the nature of simulation. See text for details.

4 RESULTS

One of the objectives of this paper is to study morphological evolution in simulated and optical clusters using M (equation 4) and ϵ (equations 5–7) as quantitative measures. These parameters represent the shape characteristics of a set of iso-density/intensity contours corresponding to a set of density/brightness levels. The levels represent equal interval in area, i.e. size in log space, which allow higher resolution and hence higher weight to the dense, central region.

In this study, we emphasize the morphological properties of the dense, central region of clusters. We analyse each cluster at two different threshold levels corresponding to radii $\sim$0.5 and $\sim 1\,h^{-1}$ Mpc where the outer radius is within approximately three times the core radius (Bahcall 1999). For each radius, measurements are relative to the centre.

Cluster images are smoothed by a Gaussian filter with a smoothing scale (SS) $\sim 50\,h^{-1}$ kpc. We choose this scale after trials with different values. Our experience shows that for a scale smaller than $\sim 50\,h^{-1}$ kpc, images contain too much noise whereas for a larger scale they become over smoothed. We note that smoothing affects the gross morphology without much distortion in the evolutionary trend of the parameters. The trend holds for both simulated and observed cluster samples.

In Figs 6 and 7, we show detailed properties of adiabatic and observed clusters using $\bar{M}_{\rm eff}$ and $\bar{\epsilon}_{\rm agg}$. These figures show results for SS $= 50\,h^{-1}$ kpc within a radius of $0.5\,h^{-1}$ Mpc (panels numbered 1)

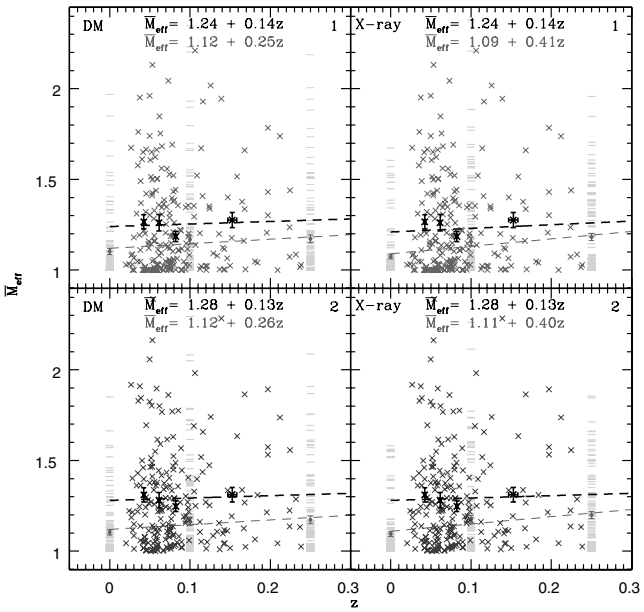

Figure 6. A detailed comparison of the estimate of $\bar{M}_{\rm eff}$ for the adaibatic DM (left-hand panels) and X-ray (right-hand panels) clusters and the optical sample with SS $= 50\,h^{-1}$ kpc within $0.5\,h^{-1}$ Mpc (Panel 1) and $1.0\,h^{-1}$ Mpc (Panel 2) radius. Simulated clusters are shown by (faint) horizontal lines at $z = 0.25, 0.10, 0.0$, and the optical clusters are shown by (dark) crosses. The expressions represent the best-fitting lines for observation (dark; top line in each panel) and simulation (faint; second line in each panel).

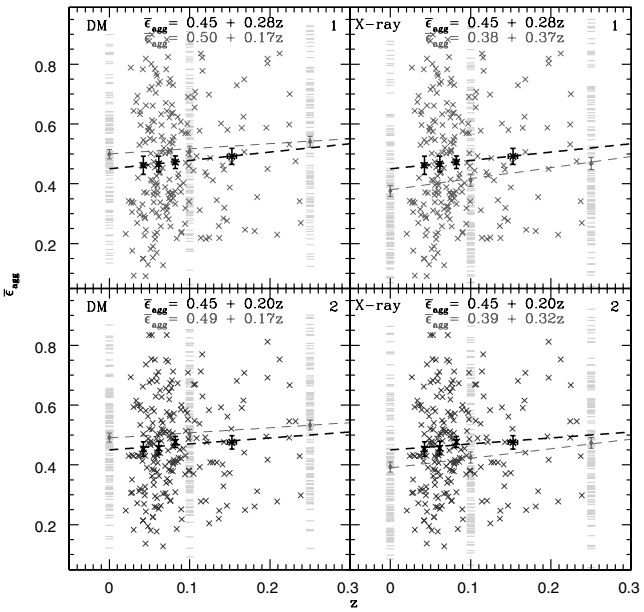

Figure 7. A detailed comparison of the estimate of $\bar{\epsilon}_{\rm agg}$ obtained from the adaibatic DM (left-hand panels) and X-ray (right-hand panels) clusters and from the optical sample. Presentation style is similar to Fig. 6.

and 1 h^{-1} Mpc (panels numbered 2). Simulated clusters are shown by (faint) horizontal lines at three different redshifts, and the optical clusters are shown by (dark) crosses. The expressions at each panel represent the best-fitting line relating the mean of the parameter to the redshift, although we note that at each redshift the distribution functions are highly non-Gaussian. An interesting feature of these figures is that, at least within $z \leqslant 0.25$, optical clusters have similar dispersion in both $\bar{M}_{\rm eff}$ and $\bar{\epsilon}_{\rm agg}$. Similar behaviour is also noted for other parameters in this redshift range, irrespective of simulation types. The wide spread in multiplicity and projected shape of DM haloes and X-ray gas is a clear reflection of different merging history (Jing & Suto 2002). Note that the error bar in the normalizations (i.e. intercepts) of the best-fitting lines is less than 10 per cent for all parameters (not shown in these figures).

We quantify the rate of evolution by the slope of the best-fitting line where the rate means either $\mathrm{d}M/\mathrm{d}z$ or $\mathrm{d}\epsilon/\mathrm{d}z$. For gross morphology, we refer to the normalization of this line. We present our final results in Figs 8–13 within $\sim$0.5 and $\sim 1\,h^{-1}$ Mpc radii with SS $\sim 50\,h^{-1}$ kpc both for simulated and for optical samples. For simulations, we show the best-fitting line along with its expression in grey colour. We divide the optical sample into four bins with equal number of clusters in each bin. In this case, the best-fitting line is shown in dark colour. No expression is given for this line. In both simulated and observed clusters, the error bar represents the error in the mean.

4.1 Comparison among simulated cluster samples

A visual examination of Figs 8–13 clearly shows an evolutionary trend in cluster morphology since the gross properties of clusters indeed change with redshifts. We are interested in determining the significance of this trend of cluster properties computed at two different regions surrounding the cluster centre, and then to compare it with observations.

Cluster properties within $\sim 0.5\,h^{-1}$ Mpc of the different samples are shown in Figs 8–10. In terms of multiplicity, a parameter that probes the number of subcomponents present in a complex system, we find that cooling samples have slightly higher value of multiplicity at all redshifts compared to that in the adiabatic sample. The low

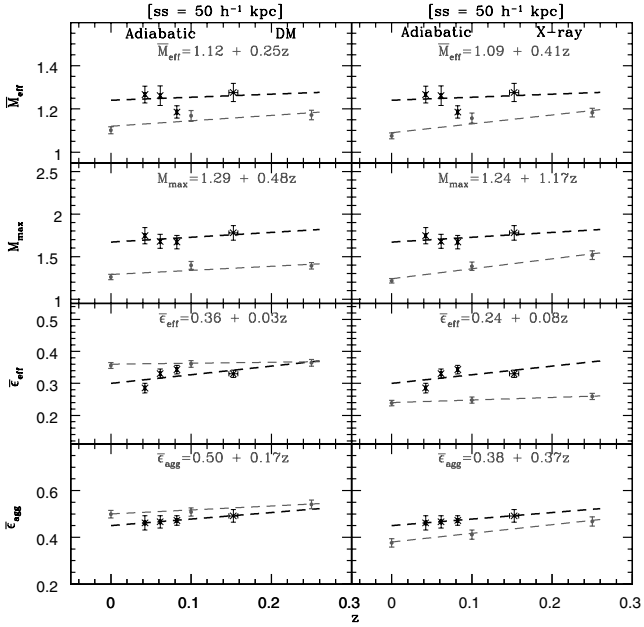

Figure 8. Adiabatic sample with $50\,h^{-1}$ kpc SS within $0.5\,h^{-1}$ Mpc radius. Dark and grey lines are used for optical and simulated clusters, respectively. The error bar represents the error in the mean. The expression at each panel relates the evolution of the mean value of the parameter of with redshift. The strength of evolution for optical clusters is $\mathrm{d}\bar{M}_{\rm eff}/\mathrm{d}z \sim 0.14$, $\mathrm{d}M_{\rm max}/\mathrm{d}z \sim 0.57$, $\mathrm{d}\bar{\epsilon}_{\rm eff}/\mathrm{d}z \sim 0.27$ and $\mathrm{d}\bar{\epsilon}_{\rm agg}/\mathrm{d}z \sim 0.28$.

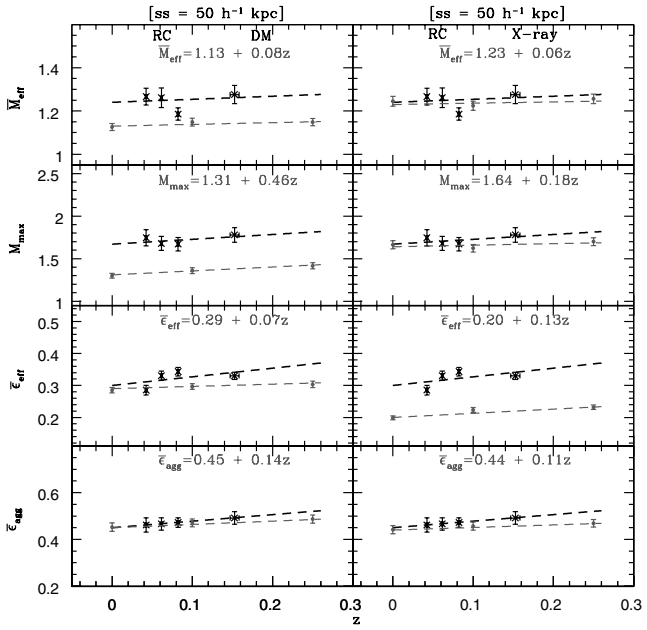

Figure 9. RC sample with 50 h^{-1} kpc SS within 0.5 h^{-1} Mpc radius. Presentation style is similar to that of Fig. 8.

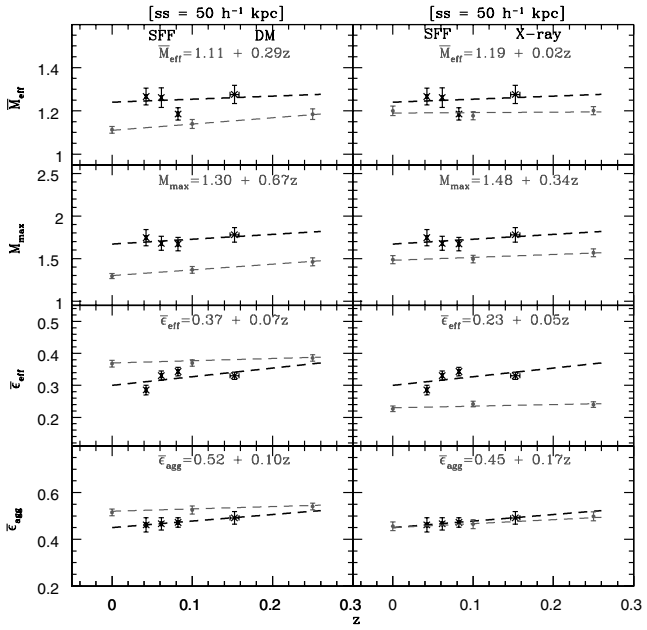

Figure 10. SFF sample with 50 h^{-1} kpc SS at 0.5 h^{-1} Mpc radius. Presentation style is similar to that of Fig. 8.

abundance of single-component systems with RC indicates that the dense, cool core substructures are long-lived features (Motl et al. 2004). We find that the feedback mechanism with cooling makes cosmological systems less clumpy than systems without feedback. Energy feedback process, most likely, slows down the rate of evolution in the X-ray clusters than those in the cooling only samples. However, this is quite opposite for the DM haloes. Higher multiplicity in the X-ray clusters in the cooling samples indicates a possibility of less-efficient merging in hot baryonic gas.

In all simulations, multiplicity shows a clear trend with redshift: clusters have higher (mean) multiplicity at higher redshifts. Cluster

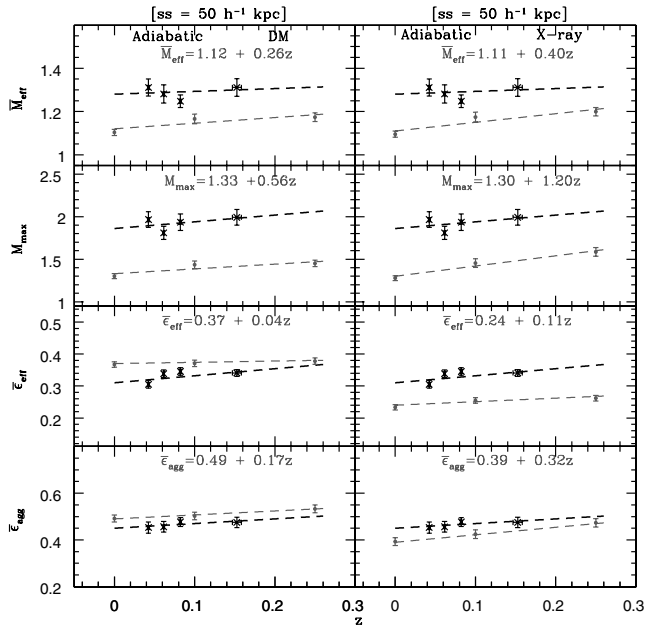

Figure 11. Adiabatic sample with 50 h^{-1} kpc SS within 1.0 h^{-1} Mpc radius. Presentation style is similar to that of Fig. 8. The strength of evolution for optical clusters is $d\bar{M}_{eff}/dz \sim 0.13$, $dM_{max}/dz \sim 0.79$, $d\bar{\epsilon}_{eff}/dz \sim 0.22$ and $d\bar{\epsilon}_{agg}/dz \sim 0.20$.

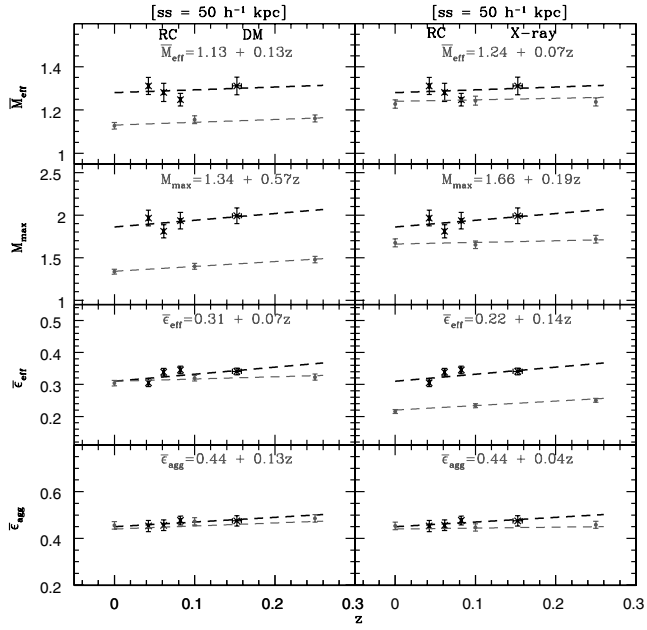

Figure 12. RC sample with 50 h^{-1} kpc SS within 1.0 h^{-1} Mpc radius. Presentation style is similar to that of Fig. 8.

multiplicity reflects substructure's merger rate. It decays by the rate at which the cluster can relax, a time-scale which is roughly equal to the dynamical time. The CDM haloes host a larger amount of substructure at higher redshifts because of lower accretion time as compared to the dynamical time (see Zentner et al. 2005). This is the reason for the systematic increase in overall substructures with increasing redshifts.

In terms of ellipticity, we find that the X-ray clusters, in general, are more regular than the haloes. The X-ray emitting hot gas

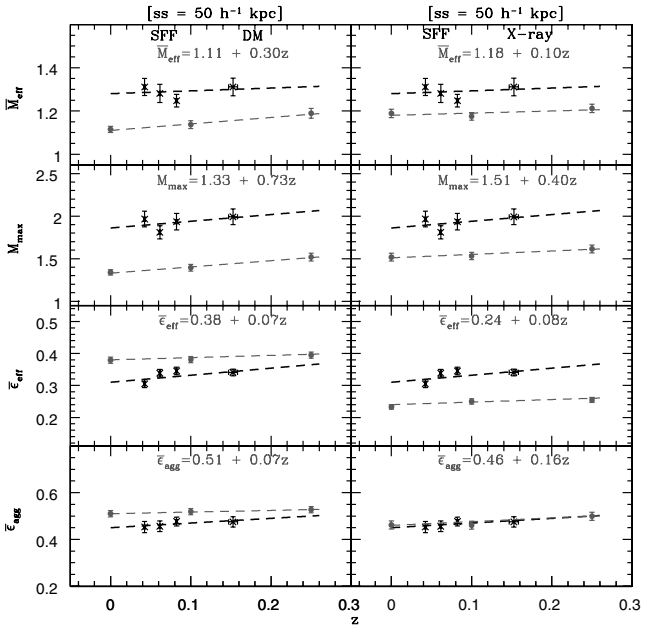

Figure 13. SFF sample with 50 h^{-1} kpc SS within 1.0 h^{-1} Mpc radius. Presentation style is similar to that of Fig. 8.

is supported by the thermal pressure. Due to its isotropic pressure support, the X-ray gas becomes homogeneously distributed in the background DM potential where it evolves. As a result, morphology of the distribution of X-ray gas appears more regular. Our results suggest that in X-ray clusters the irregular subcomponents are distributed over a region instead of making a filamentary structure along one direction. A comparison of $\bar{\epsilon}_{\rm eff}$ with $\bar{\epsilon}_{\rm agg}$ for the haloes (in all samples) shows that the halo subclumps are not distributed uniformly around the central region. Rather, these clumps are spread out mostly in one direction forming filamentary structure, as indicated by the larger value of $\bar{\epsilon}_{\rm agg}$.

No significant evolution is signalled by $\bar{\epsilon}_{\rm eff}$ for the DM clusters in any of these samples. Recall that this parameter is an indicator of shapes of individual components in a cluster. Therefore, no evolution means that shapes of isolated components in clusters at one redshift appear similar at any other redshifts. Since it places emphasis on individual component, therefore, it is not unusual to find no evolution quantified by this parameter. However, shapes of subclumps in the distributions of X-ray gas change in the cooling simulations compared to other simulations.

Properties of simulated clusters within $\sim 1\,h^{-1}$ Mpc are shown in Figs 11–13. We note that in this distance, small-scale structures of simulated clusters do not change significantly than what we find in smaller scale. This implies that the small subclumps can exist up to a Mpc scale, and could be distributed widely over the cluster body. However, in this scale substructures evolve a bit faster. We find that individual, isolated components become a bit more flattened, and their evolution is slightly stronger. The overall shape of the clusters, however, is less flattened than the central region, and evolution is weak in all simulations.

We take projections along each axis at a time and repeat our analysis. Recall that in this case, each subsample (along each axis) has only 41 clusters. The analysis of these subsamples does not show significant variation from the primary sample. Therefore, it is unlikely that the overall result may have contaminated by the projection effect. We have also repeated our analysis using different values for the density/brightness levels. Apart from a minor change in gross morphology, we find similar results for the rate of evolution.

We summarize our main results as follows. First, the DM haloes show very similar evolution in all samples of clusters. Secondly, the X-ray clusters in the adiabatic simulation evolve faster than those with RC. Thirdly, morphology of the central parts of clusters evolves slightly strongly than the outer regions. Finally, feedback processes with cooling makes the DM haloes slightly more flattened and slower in evolution than the cooling only simulations [see Kazantzidis et al. (2004) for a similar trend].

We emphasize that the measured quantities for the DM distributions in all the three samples are very similar. This is a check on the consistency of the simulations and analysis. The result is expected as the *N*-body segment of the simulations is identical in all the three cluster samples with the exception of the gas that makes a relatively minor contribution to the total gravitational potential. The LSS of adiabatic and cooling clusters is generally similar, but their small-scale structures are determined by the overall cluster properties rather than perturbative interactions (Motl et al. 2004). In the adiabatic clusters, the mixing of in-falling subclumps into the main cluster medium is quicker relative to the RC clusters where substructures can be long lived. This is a reason behind the fast evolution of adiabatic X-ray clusters. The relaxation time-scale for collisionless particles is much longer than that of the collisional gas particles (Frenk et al. 1999; Valdarnini et al. 1999). Therefore, the DM haloes will appear not only more elongated than the distributions of X-ray gas, but the redshift evolution of their shapes will also be slower. More spherical configurations for X-ray clusters are also expected from the point of view that intracluster gas is approximately in hydrostatic equilibrium and is supported by isotropic pressure (Sarazin 1988). The DM, on the other hand, appears to be distributed like galaxies as indicated by recent observations from gravitational lensing (Fischer & Tyson 1997; Fischer et al. 1997; Kochanek 2002; Hoekstra 2003; Hoekstra, Yee & Gladders 2004) and by high-resolution hydrodynamical simulations (Kang et al. 2005; Nagai & Kravtsov 2005; Maccio et al. 2006).

There is a consensus based on the observations of X-ray clusters that cooling affects the mass distribution appreciably only in the inner ∼10 per cent of the virial radius of cluster size haloes (Sarazin 1988). Contrary to that, recent high-resolution hydrodynamic simulations show something quite interesting (see Kazantzidis et al. 2004). Kazantzidis et al. show that there is a significant difference in overall shape between dissipationless and dissipative simulations, which is persistent up to the virial radius. The virial mass of their DM haloes ranges from $\approx 10^{13}$ to $3 \times 10^{14}\,h^{-1}\,{\rm M}_{\odot}$ which translates to the virial radius range ∼0.26–0.82 h^{-1} Mpc assuming $\Delta_{\rm vir}(z = 0) \sim 337$, $h \sim 0.7$ and $\rho_c \sim 1.87\,h^2 \times 10^{-29}\,{\rm g\,cm^{-3}}$ (Kolb & Turner 1990; Zentner et al. 2005). Kazantzidis et al. present their analysis up to the virial radius. However, from the trend seen right at the virial radius, it seems likely that it goes a bit further down along the radial direction before shapes in dissipative and dissipational simulations converge.

The baryon fraction ($\Omega_{\rm b} \sim 0.043$) in Kazantzidis et al. simulations is larger than that which has been used in our simulations. Therefore, question can be raised whether low baryon density can also produce systematic shift in the shapes of DM haloes to be robust on scales of Mpc as noted in our work. Our simulations use baryon density ($\Omega_{\rm b} = 0.026$) and normalization of fluctuation spectrum ($\sigma_8 = 0.928$) which are slightly off than the corresponding *Wilkinson Microwave Anisotropy Probe* (*WMAP*) values ($\Omega_{\rm b} = 0.044$ and

$\sigma_8 = 0.84$; Spergel et al. 2003). Baryon density is an important cosmological parameter which affects RC and X-ray luminosity at the central region of large virialized structures. Higher Ω_b enhances the cooling rate, subsequently making the central region more regular (Sarazin 1988; Kazantzidis et al. 2004; Springel et al. 2004; Allgood et al. 2005; Flores et al. 2005). Recent numerical simulations show that larger σ_8 produces DM haloes that are more regular in the central regions (Allgood et al. 2005). Therefore, we note that cooling is underemphasized while the core DM substructure is overemphasized in our simulations. It may be likely that the offset of Ω_b and σ_8 compared to *WMAP* would balance each other, and our results obtained from the cooling simulations would still be representative had we been using the *WMAP* values.

With cooling only, our simulated clusters of galaxies show a large amount of long-lived substructure compared to the other simulated samples. While the amount of cooling in this sample is unphysical, it represents an interesting, theoretical, limiting case. On the scale of the cluster itself, the gravitational and dynamical effects of cool, dense cores of gas have significantly altered the shape of the clusters to length-scales comparable to the virial radius (see Figs 4 and 5). The perturbation from cool baryonic clumps may thus significantly alter model-dependent mass maps derived from weak lensing studies. The robust substructures present in the cooling only sample may also play a role in steepening the total cluster mass profile (Maccio et al. 2006), and higher resolution simulations may bound the possible contribution of substructures to strong lensing in clusters. Though beyond the scope of the current paper, these connections to lensing studies will be pursued in future work.

Numerical simulations provide interesting information on two different aspects of the LSS: (1) shape of the central structures in galaxy or cluster size haloes and (2) change in shape of haloes with radial distance, irrespective of the nature of simulation. Recent high-resolution hydrodynamical simulations have quite successfully shown that hydrodynamical phenomena make cluster centres considerably more spherical than those in the adiabatic simulations. However, radial dependence of shape is still a controversial issue. While Frenk et al. (1988), Bullock (2002), Springel et al. (2004), Hopkins, Bahcall & Bode (2005) and hydrosimulation of Kazantzidis et al. (2004) agree that inner part of clusters is more spherical than the outer part, the following groups of Dubinski & Carlberg (1991), Warren et al. (1992), Jing & Suto (2002), Allgood et al. (2005), and hydrosimulation of Tissera & Dominguez-Tenreiro (1998) find it completely opposite. Our results closely follow the latter group.

Note that radial dependence of shape is not monotonic. It changes in a quite complicated way depending on the presence of subclumps as one can see from Fig. 5. A similar trend is also seen in hydrosimulations of Kazantzidis et al. (2004)

4.2 Comparison with optical clusters

We have analysed a sample of ACO clusters within redshift, $z \leqslant 0.25$. The sample contains 208 optical clusters derived from 10-inch photographic plates taken with the 48-inch Palomar Schmidt Telescope. For details of the data acquisition and processing, see Trèvese et al. (1992), Flin et al. (1995), Trèvese et al. (1997) and Flin et al. (2000). Results obtained from the optical clusters are shown in Figs 8–13 using dark dashed lines. The summary of our results is as follows.

(i) The optical clusters are, in general, more clumpy than the simulated DM haloes as given by both $\bar{M}_{\rm eff}$ and $M_{\rm max}$. The substructure at the central part of X-ray clusters in the RC sample is compatible with the optical clusters, at least, within redshift $z \leqslant 0.25$. At large radius, the optical clusters include more small-scale structures and show stronger evolution in substructures.

(ii) The substructures of hot baryonic gas evolve much strongly in the adiabatic simulation than that in the galaxy distribution ($\mathrm{d}\bar{M}_{\rm eff}/\mathrm{d}z \sim 0.14, 0.13$ in 0.5 and 1 h^{-1} Mpc). On the other hand, effective subclumps ($\bar{M}_{\rm eff}$) of the haloes have faster rate in both adiabatic and SFF simulations. Feedback process along with RC makes rapid evolution in DM halo structures. In terms of $M_{\rm max}$, however, evolution of the galaxy distribution is always stronger compared to all the three simulations ($\mathrm{d}M_{\rm max}/\mathrm{d}z \sim 0.57, 0.79$ for 0.5 and 1 h^{-1} Mpc, respectively).

(iii) The largest component of the DM haloes (probed by $\bar{\epsilon}_{\rm eff}$) in the adiabatic and SFF simulations has higher elongation compared to that in the galaxy distribution. In the RC simulation, we find an opposite trend. The shape of the largest subclump formed in the distributions of X-ray emitting hot gas in all the three simulations is significantly rounder than that of the optical clusters ($\mathrm{d}\bar{\epsilon}_{\rm eff}/\mathrm{d}z \sim 0.27, 0.22$ in 0.5 and 1 h^{-1} Mpc, respectively).

(iv) The overall shape (probed by $\bar{\epsilon}_{\rm agg}$) and the strength of evolution in optical clusters ($\mathrm{d}\bar{\epsilon}_{\rm agg}/\mathrm{d}z \sim 0.28, 0.2$ in 0.5 and 1 h^{-1} Mpc, respectively) show nice agreement with that of the X-ray clusters in dissipative simulations. In dissipationless simulation, however, hot gas is systematically less elongated but evolves much strongly than the galaxy distribution ($\mathrm{d}\bar{\epsilon}_{\rm agg}/\mathrm{d}z \sim 0.28, 0.2$ in 0.5 and 1 h^{-1} Mpc, respectively).

(v) The shapes of the optical clusters are comparable to the haloes only in the RC simulation. The haloes are slightly more flattened and slower in evolutionary process compared to the galaxy distributions in the adiabatic case and in simulation including feedback processes with cooling.

(vi) The strength of shape evolution given by $\mathrm{d}\bar{\epsilon}_{\rm agg}/\mathrm{d}z$ is slightly stronger around the cluster core, in both observed and simulated clusters.

There are several possibilities for optical clusters to be more clumpy. First, the choice of smoothing may not be optimal for the optical sample. The SS used in our study, therefore, should be taken as the lower limit. Secondly, projection effect due to the background galaxies may also play an important role. This effect becomes significant as one moves away from the clusters centre (Kolokotronis et al. 2001). Thirdly, since ACO clusters are selected via richness criteria and it has been shown that richness is poorly correlated with mass (Girardi et al. 1998; Miller, private communication), there is a chance that optical sample may be biased towards high mass end of cluster mass range or clusters that have gone through recent merger. Massive clusters are dynamically less relaxed and hence rich in substructure. Well-defined mass selection criteria need to be applied for a more systematic comparison as recent numerical simulations show that cluster shapes depend on mass, although the mass–shape correlation is weak and show large dispersion (Bullock 2002; Jing & Suto 2002; Allgood et al. 2005; Hopkins et al. 2005).

Regarding the comparison of the strength of evolution, we note that the morphological parameters derived for the set of simulated haloes have uniform statistical weight at all redshifts. However, this is certainly not the case for the observed sample as it has considerably more weight towards $z = 0.0$ than the simulated samples (see Figs 6 and 7). As mentioned earlier, the scatter is comparable in both samples, and therefore we believe the choice of binning has less effect on the overall outcome of our analysis.

4.3 Results from previous studies on observed clusters

In this section, we summarize the results obtained from previous studies on optical and X-ray clusters. Our objective is to highlight the fact that different samples of clusters give different rates of evolution in cluster morphology. Due to the methodological differences, we refrain from making a direct comparison with the results of these studies.

To find cluster shapes, all previous studies follow the procedure described in Carter & Metcalfe (1980). These studies, however, differ in adopting weighting factor, threshold level, cluster centre and smoothing techniques to construct galaxy density distribution from spatial distribution. It is also important to note that cluster shape quantified by ellipticity is not uniquely defined. Therefore, to help the reader get a better feel of the inherent differences of previous studies, we also provide a brief outline of the methodologies used in these studies.

The optical sample of MCM contains 138 ACO clusters with $z < 0.1$ which has been compiled from West & Bothun (1990), Rhee, van Haarlem & Katgert (1991) and Kolokotronis et al. (2001). This sample shows no significant evolution, $\mathrm{d}\epsilon/\mathrm{d}z \sim 0.03$.

The former two groups measure cluster shapes from discrete galaxy distribution using method of moments. They define the two-dimensional moments as

$$\mu_{mn} = \frac{\sum_{i,j} (x_i - x_0)^m (y_j - y_0)^n}{N}, \tag{8}$$

where x_0, y_0 are the coordinates of the brightest galaxy taken as the cluster centre, and N is the total number of galaxies within the region which is 3σ above the background noise and m, $n = 0$, 1, 2. They diagonalize the matrix formed by the components μ_{20}, μ_{02} and μ_{11}, find the eigenvalues and obtain cluster shape using eigenvalues from the relation, $\epsilon = 1 - \lambda_2^2/\lambda_1^2$, where $\lambda_1 > \lambda_2$. Kolokotronis et al. (2001) use moment of inertia method for a sample containing 22 automated plate measurement (APM) clusters along with their *ROSAT* counterparts in the redshift range, $z \leqslant 0.13$. They use Gaussian smoothing on galaxy density distribution and define the components of the symmetric inertia tensor as

$$I_{11} = \sum_i w_i (r_i^2 - x_i^2),\ I_{22} = \sum_i w_i (r_i^2 - y_i^2),$$

$$I_{12} = I_{21} = -\sum_i w_i x_i y_i, \tag{9}$$

where w_i is the average cell density within 0.75 h^{-1} Mpc region and $r_i^2 = x_i^2 + y_i^2$. After defining inertia tensor, Kolokotronis et al. follow similar route to the other groups to define shape except that they define ellipticity as $\epsilon = 1 - \lambda_2/\lambda_1$.

Plionis (2002) analyse the largest sample of optical clusters following the method used in Kolokotronis et al. (2001). His sample has 407 APM clusters within a volume of $z < 0.18$. The rate of evolution for the Plionis sample is $\mathrm{d}\epsilon/\mathrm{d}z \sim 0.7$. However, if both are combined, replacing the common ones by the APM clusters, the rate increases. The combined sample of ∼500 optical clusters with $z < 0.18$ shows $\mathrm{d}\,\epsilon/\mathrm{d}z \sim 1.06$.

It is rare to find a large sample of X-ray clusters with up-to-date ellipticity measurements. The X-ray sample of MCM is compiled from Mcmillan, Kowalski & Ulmer (1989; hereafter MKU) and Kolokotronis et al. (2001). MKU measure cluster shape using the method of moments from two-dimensional X-ray surface brightness images. They adopt the following definition of the moment,

$$\mu_{mn} = \frac{\sum_{i,j} f_{ij} (x_i - x_0)^m (y_j - y_0)^n}{\sum_{ij} f_{ij}}, \tag{10}$$

where x_0, y_0 are the components of the image centroid, $x_0 = \sum x_i f_{ij} / \sum f_{ij}$ and $y_0 = \sum y_j f_{ij} / \sum f_{ij}$. They determine the overall shape of a cluster using the faintest flux level available for that object. This sample has 48 clusters with $z < 0.1$ which is three times smaller than the MCM optical sample and an order of magnitude smaller than the APM sample. It also has a lower redshift limit than the APM sample. The rate of evolution for this sample is $\mathrm{d}\epsilon/\mathrm{d}z \sim 1.7$. The result suggests faster evolution for the X-ray clusters than the optical one. Interestingly, a comparison of optical and X-ray clusters within Kolokotronis et al. (2001) sample shows completely opposite trend: galaxy density distributions have stronger evolution than the distribution of hot gas. The galaxy and X-ray cluster shapes follow a trend where flattened gas distribution signals anisotropic distribution of galaxies. However, the scatter is large in both relationships. It is not clear to us what could be the reasons of possible contradictions except the fact that MCM sample is most likely contaminated due to different methodologies. Besides, it is also difficult to make any definite conclusion because of the smaller sizes of the samples. A large sample of X-ray clusters with better selection criteria and extended to higher redshift are needed.

We reanalyse $\epsilon - z$ estimates derived from the APM cluster data and the combined sample imposing a redshift cut-off $z < 0.1$ in order to be consistent with the redshift range of MCM X-ray sample. For these samples, we find the rate of evolution as, $\mathrm{d}\epsilon/\mathrm{d}z \sim 1.02$ and ∼1.0, respectively. We find that evolution of optical clusters accelerates in this redshift range, but it is still slower than that of the X-ray.

Flin, Krywult & Biernacka (2004; hereafter FKB) have analysed a sample of 246 ACO clusters for $z \leqslant 0.31$. This group uses the same definition of moment as in equation (1). They use density peak as the cluster centre and measure shapes at different circular aperture radii ranging from 0.5 to 1.5 h^{-1} Mpc with an increment of 0.25 h^{-1} Mpc. They estimate cluster shape at all radii and find no dependence of cluster ellipticity on redshift. Interestingly, FKB noted a decrement of $\mathrm{d}\,\epsilon/\mathrm{d}\,z$ with radius. They find positive evolution at radii of 0.5 and 0.75 h^{-1} Mpc. However, for radii $\geqslant 1\,h^{-1}$ Mpc, they report negative evolution. The mean of their estimates derived from these five radii shows $\bar{\epsilon} \approx 0.22$ and $\mathrm{d}\bar{\epsilon}/\mathrm{d}z \sim 0.013$. For $z < 0.1$, their result also indicates weak evolution. We use this sample of optical clusters for our analysis (see Section 4.2) but with a reduced number (208) of clusters. The reduction is made after visual inspection, and it is due to the removal of cluster images that appear either small or close to the boundary.

It should be noted that MCM and APM samples emphasize cluster morphology in two different regions. The MCM sample excludes any study with radius less than 1 h^{-1} Mpc and includes the estimate of ellipticity within ∼1–2 h^{-1} Mpc from the cluster centre. The APM sample, however, provides information on cluster shape within 0.75 h^{-1} Mpc of the centre. Therefore, care must be taken in interpreting and comparing results of observed clusters with simulations if both are not analysed under the same measurement technique. Unfortunately, the studies of Floor et al. (2003) and FMM have ignored this fact.

In spite of differences in the evolution of cluster morphology, optical samples are consistent with one another at least in one case: shape of galaxy density distributions evolves strongly in the central region (Plionis 2002) than in the outer part (MCM). Interestingly, our results are also consistent with this trend. For X-ray clusters, this trend has yet to establish.

5 CONCLUSIONS

Numerical simulations provide a unique opportunity to follow the hierarchical nature of the LSS formation in both linear and non-linear

regimes (Frenk et al. 1985, 1988; Quinn, Salmon & Zurek 1986; Efstathiou et al. 1988). In order to be representative of the reality, results from simulations should agree with observations. Observations provide evidence of morphological evolution in galaxy clusters (MCM; Plionis 2002; Jeltema et al. 2005). Simulations should also show a similar trend. Besides, in the CDM model luminous galaxies are associated with the DM subhaloes which reside in bigger parent haloes, closely associated with galaxy clusters. According to this model, statistical properties of galaxies, e.g. mass, substructure, shape, etc., would show a similar trend to that of the subhaloes while X-ray emitting hot gas would have different properties than galaxies and subhaloes. A statistical analysis of various properties of haloes, galaxy clusters and X-ray gas could provide clues to find possible biasing of luminous galaxies towards DM subhaloes and whether or not they have any correspondence with the distribution of hot gas. With this in mind, we have studied redshift evolution of cluster morphology simulated, respectively, in the adiabatic limit, with RC and with star formation including supernovae feedback at three different redshifts, $z = 0.0$, 0.10 and 0.25. For comparison, we have also studied a sample of observed clusters containing 208 ACO clusters within redshift, $z \leqslant 0.25$.

Since observed clusters are projected along the line of sight and lack the full three-dimensional information, therefore we use projected simulated clusters. Each cluster image is an $8\,h^{-1}$ Mpc frame containing 360×360 pixels. Clusters are analysed at two different density/brightness threshold levels corresponding to radii 0.5 and $1\,h^{-1}$ Mpc from the cluster centre. To quantify morphological evolution, we use multiplicity and ellipticity as two different probes that are sensitive to cluster substructures and shape.

Our results indicate that optical clusters have, in general, more substructures than simulated haloes and X-ray brightness distributions. Cluster components, in both observed and simulated clusters, evolve with redshifts, and the evolution is different at different regions from cluster centres. In terms of total multiplicity ($M_{\max}$), observed clusters have stronger evolution compared to DM haloes. The X-ray brightness distributions, however, show steeper evolution (than that of galaxy clusters) in dissipationless simulation.

We find that in terms of overall shape, simulations do model the observed universe in an interesting way. The simulated clusters evolve with redshift, consistent with the hierarchical formation scenario. However, observed clusters appear to be slightly more flattened at higher redshift than the simulated one indicating slower evolution in simulated objects. This may reflect some form of incompleteness in our understanding in simulating the LSS. Our results differ from those of FMM, who reported that the evolution in the simulated cluster shape is significantly slower than the observed one. We not only find stronger structural evolution in simulated clusters, but also find that observed cluster shapes appear to be consistent with dissipative simulations, at least, in the redshift range $z < 0.1$. The discrepancies noted in FMM is due to the different redshift range probed as well as intrinsic methodological differences while comparing simulations with observations.

We note that on one hand shapes of optical clusters seem to be compatible with both the haloes and X-ray brightness distributions, one the other hand, both of these components appear to be less clumpy than the distribution of galaxies. Therefore, it seems puzzling whether or not there is any correspondence between the DM haloes and galaxies. The existence of any such correspondence is still a matter of ongoing debate as there are conflicting results based on systematics of numerical simulations such as the nature of simulations (dissipationless or dissipative) and the effect of mass and force resolution (see Maccio et al. 2006). In the context of the CDM model, we would expect that the optical clusters would have similar morphology and evolutionary trend to that of the haloes and would be different from the properties of the distribution of hot gas traced in the X-ray region of the spectrum.

Within the uncertainties and systematics involved in our optical sample, the results indicate that the properties of optical clusters do not exactly represent the distribution of either the haloes or the X-ray emitting gas in any of the simulations. We find offsets in the measured parameters, such as multiplicities and ellipticities, between observations and simulations are unable to find any clear signature of DM galaxy biasing based on our morphological analysis. This may be an indication, although in no way conclusive, of the fact that these components of the LSS may represent intrinsically different populations, and galaxies may not trace the DM distributions (see Gao et al. 2004a,b; Nagai & Kravtsov 2005). However, this is merely a speculation, and we stress that care must be taken in interpreting our results as one must be careful in selecting proper measures, radius, mass range and, most importantly, well-defined samples of clusters to have unbiased and meaningful results in any morphological analysis comparing observations and simulations.

We find that the measurements from different samples do not agree on the evolution rate. Take, for example, optical clusters with $z < 0.1$, and radius, $0.75\,h^{-1}$ Mpc. In this case, the APM sample shows $\mathrm{d}\epsilon/\mathrm{d}z \sim 1.02$. FKB, on the other hand, finds much weaker evolution, $\mathrm{d}\epsilon/\mathrm{d}z \sim 0.2$. As mentioned in FKB, the discrepancy may be due to differences in adopting cluster centres, smoothing and applied method of shape determination.

A preliminary analysis of a sample of 800 clusters constructed from the Sloan Digital Sky Survey (SDSS) shows that ellipticity evolution of optical clusters, for $z < 0.1$ and within $\sim 1\,h^{-1}$ Mpc, is weaker than that of the APM clusters. The result indicates that clusters with different mass limits evolve differently. Large, massive clusters ($M \sim 10^{15}\,\mathrm{M}_{\odot}$) have stronger evolution compared to the less massive clusters ($M \sim 10^{13}$–$10^{14}\,\mathrm{M}_{\odot}$) (Miller, private communication). This is an interesting observation. If it is confirmed, then the scaling relation between axes ratio and mass noted in simulations (Bullock 2002; Jing & Suto 2002) must be modified to be consistent with observations.

The SDSS sample is uniform with a well-documented selection function and high degree of completeness. We may then infer that the cluster samples discussed previously have less uniformity in mass range: the APM catalogue and FKB samples are biased towards massive clusters, whereas the MCM samples contain more less massive clusters. The discrepancy may also arise from the techniques applied in ellipticity estimates [see also Flores et al. (2005) in this regard]. Unfortunately, we are unable to check the evolution strength–mass relation for our optical sample because, apart from an approximate range, no well-defined criteria have been used to sort clusters into different mass bins.

The discrepancy in the optical samples is an indication of different selection criteria used to construct the catalogues. Larger and more complete catalogues obtained from the SDSS and *XMM–Newton* survey may be able to shed more light on this issue. It is also likely that numerical simulations may lack crucial physics that need to be included (see FMM for discussion). In future, we will analyse clusters simulated with various gas physics, e.g. thermal conduction and AGN heating, and compare them with the SDSS clusters. The results of these studies may give us some clues to gain better insight into the current discrepancy.

ACKNOWLEDGMENTS

We thank the anonymous referee for constructive comments and criticisms which helped us improve the quality of this paper. We thank M. Plionis for providing the APM cluster ellipticity data and Scott W. Chambers for the MCM data sets. NR thanks Hume Feldman and Bruce Twarog for many useful discussions.

REFERENCES

Abell G. O., Corwin H. G., Olowin H. G., 1989, ApJS, 70, 1 (ACO)
Allgood B., Flores R. A., Primack J. R., Kravtsov A. V., Wechsler R. H., Faltenbacher A., Bullock J. S. 2005, MNRAS, in press (doi:10.1111/j.1365-2966.2006.10094.x) (astro-ph/0508497)
Aninos P., Norman M. L., 1996, ApJ, 459, 12
Bahcall N. A., 1999, in Dekel A., Ostriker J. P., eds, Formation of Structure in the Universe. Cambridge Univ. Press, New York, p. 135
Beisbart C., 2000, PhD thesis, Ludwig Maximilians Universität, Münichen, Germany
Beisbart C., Buchert T., Wagner H., 2001, Physica A, 293, 592B
Beisbart C., Valdarnini R., Buchert T., 2001, A&A, 379, 412
Bullock J. S., 2002, in Natrajan P., ed., The Shapes of Galaxies and Their Dark Matter Halos. World Scientific Press, Singapore, p. 109
Buote D. A., Tsai J. C., 1995, ApJ, 452, 522
Buote D. A., Jeltema T. E., Canizares C. R., Garmire G. P., 2002, ApJ, 577, 183
Carter D., Metcalfe N., 1980, MNRAS, 191, 325
Cen R., Ostriker J. P., 1992, ApJ, 393, 32
Chandran B. D. G., Cowley S. C., 1998, Phys. Rev. Lett., 80, 3077
Colella P., Woodward P. R., 1984, J. Comput. Phys., 54, 174
Crone M. M., Evrard A. E., Richstone D. O., 1996, ApJ, 467, 489
Dubinski J., 1994, ApJ, 431, 617
Dubinski J., Carlberg R. G., 1991, ApJ, 378, 496
Efstathiou G. P., Frenk C. S., White S. D. M., Davis M., 1988, MNRAS, 325, 715
Eisenstein D. J., Hut P., 1998, ApJ, 498, 137
Fischer P., Bernstein G., Rhee G., Tyson J. A., 1997, AJ, 113, 521
Fischer P., Tyson J. A., 1997, AJ, 114, 4
Flin P., Trèvese D., Cirimele G., Hickson P., 1995, A&AS, 110, 313
Flin P., Krywult J., Trèvese D., Cirimele G., Hickson P., 2000, A&ASS, 146, 373
Flin P., Krywult J., Biernacka M., 2004, astro-ph/0404182 (FKB)
Floor S. N., Melott A. L., Miller C. J., Bryan G. L., 2003, ApJ, 591, 741
Floor S. N., Melott A. L., Motl P. M., 2004, ApJ, 611, 153 (FMM)
Flores R. A., Allgood B., Kravtsov A. V., Primack J. R., Buote D. A., Bullock J. S., 2005, MNRAS, submitted (astro-ph/0508226)
Frenk C. S., White S. D. M., Efstathiou G. P., Davis M., 1985, Nat, 317, 595
Frenk C. S., White S. D. M., Davis M., Efstathiou G. P., 1988, ApJ, 327, 507
Frenk C. S. et al., 1999, ApJ, 525, 554
Gao L., de Lucia G., White S. D. M., Jenkins A., 2004a, MNRAS, 352, L1
Gao L., White S. D. M., Jenkins A., Stoehr F., Springel V., 2004b, MNRAS, 355, 819
Ghigna S., Moore B., Governato F., Lake G., Quinn T., Stadel J., 1998, MNRAS, 300, 146
Girardi M., Borgani S., Giuricin G., Mardirossian F., Mezzetti M., 1998, ApJ, 506, 45
Hoekstra H., 2003, MNRAS, 339, 1155
Hoekstra H., Yee H. K. C., Gladders M. A., 2004, ApJ, 606, 67
Hopkins P. F., Bahcall N., Bode P., 2005, ApJ, 618, 1
Jeltema T. E., Canizares C. R., Bautz M. W., Buote D. A., 2005, ApJ, 624, 606
Jing Y. P., Suto Y, 2002, ApJ, 574, 538
Jing Y. P., Mo H. J., Börner G., Fang L. Z., 1995, MNRAS, 276, 417
Kang X., Mao S., Gao l., Jing Y. P., 2005, A&A, 437, 383
Kazantzidis S., Kravtsov A. V., Zentner A. R., Allgood B., Nagai D., Moore B., 2004, ApJ, 611, L73
Kerscher M., Mecke K., Schmalzing J., Beisbart C., Buchert T., Wagner H., 2001a, A&A, 373, 1
Kerscher M. et al., 2001b, A&A, 377, 1
Kochanek C. S., 2002, in Natrajan P., ed., The Shapes of Galaxies and Their Dark Matter Halos. World Scientific Press, Singapore, p. 62
Kolb E. W., Turner M. S., 1990, Early Universe. Addison-Wesley Publishing Company, MA
Kolokotronis V., Basilakos S., Plionis M., Georgantopoulos I., 2001, MNRAS, 320, 49
Libeskind N. I., Frenk C. S., Cole S., Helly J. C., Jenkins A., Navarro J. F., Power C., 2005, MNRAS, 363, 146
Maccio A. V., Moore B., Stadel J., Diemand J., 2006, MNRAS, 366, 1529
McMillan S. L. W., Kowalski M. P., Ulmer M. P., 1989, ApJS, 70, 723 (MKU)
Mecke K. R., Buchert T., Wagner H., 1994, A&A, 288, 697
Melott A. L., Chambers S. W., Miller C. J., 2001, ApJ, 559, L75 (MCM)
Motl P. M., Burns J. O., Loken C., Norman M. L., Bryan G., 2004, ApJ, 606, 635
Nagai D., Kravtsov A. V., 2005, ApJ, 618, 557
Narayan R., Medvedev M. V., 2001, ApJ, 562, L129
Norman M. L., Bryan G. L., 1999, in Miyama S. M., Tomosaka K., Hanawa T., eds, ASSL Vol. 240: Numerical Astrophysics. Kluwer Academic Publishers, Boston, p. 19
Paz D. J., Lambas D. G., Padilla N., Merchin M., 2006, MNRAS, 366, 1503
Plionis M., 2002, ApJ, 572, L67
Quinn P. J., Salmon J. K., Zurek W. H., 1986, Nat, 322, 329
Rahman N., Shandarin S. F., 2003, MNRAS, 343, 933 (RS03)
Rahman N., Shandarin S. F., 2004, MNRAS, 354, 235 (RS04)
Rahman N., Shandarin S. F., Motl P. M., Melott A. L., 2004, astro-ph/0405097
Rhee G. F. R. N., van Haarlem M., Katgert P., 1991, A&AS, 91, 513
Sarazin C. L., 1988, X-ray Emission from Clusters of Galaxies. Cambridge Univ. Press, Cambridge
Schmalzing J., 1999, PhD thesis, Ludwig Maximilians Univ.
Schmalzing J., Buchert T., Melott A. L., Sahni V., Sathyaprakash B. S., Shandarin S. F., 1999, ApJ, 526, 568
Shandarin S. F., Sheth J. V., Sahni V., 2004, MNRAS, 353, 162
Spergel D. N. et al., 2003, ApJS, 148, 175
Springel V., White S. D. M., Hernquist L., 2004, in Ryder S. D., Pisano D. J., Walker M. A., Freeman K. C., eds, Proc. IAU Symp. 220, Dark Matter in Galaxies. Astron. Soc. Pac. San Francisco, p. 421
Suwa T., Habe A., Yoshikawa K., Okamoto T., 2003, ApJ, 588, 17
Thomas P. A. et al., 1998, MNRAS, 296, 1061
Tissera P. B., Dominguez-Tenreiro R., 1998, MNRAS, 297, 177
Trèvese D., Flin P., Migliori L., Hickson P., Pittella G., 1992, A&ASS, 94, 327
Trèvese D., Cirimele G., Cenci A., Appodia B., Flin P., Hickson P., 1997, A&ASS, 125, 459
Valdarnini R., Ghizzardi S., Bomometto S., 1999, New Astron., 4, 71
van den Bosch F. c., Yang X., Mo H. J., Norberg P., 2005, MNRAS, 356, 1233
Warren M. S., Quinn P. J., Salmon J. K., Zurek W. H., 1992, ApJ, 399, 405
West M. J., Bothun G. D., 1990, ApJ, 350, 36
Westbury C. F., Henriksen R. N., 1992, ApJ, 338, 64
Zentner A. R., Berlind A. A., Bullock J. S., Kravtsov A. V., Wechsler R. H., 2005, ApJ, 624, 505

This paper has been typeset from a TEX/LATEX file prepared by the author.